Electronic Supplementary Information

3,4,9,10-Perylenetetracarboxylic acid/O-phenylenediamine Nanomaterials as Novel Redox Probe for Electrochemical Aptasensor System Based on Fe_3O_4 Magnetic Bead as Nonenzymatic Catalyst

Yuanyuan Chang, Shunbi Xie, Yali Yuan, Yaqin Chai* and Ruo Yuan*

1 Experimental

1.1 Reagents and Materials

Trishydroxymethylaminomethane hydroch-loride (tris) was obtained from Roche (Switzerland). Affimag PSC Magnetic Bead (MB) was purchased from Tianjin baseline ChromTech Research Centre. Thrombin (TB), bovine serum albumin (BSA) and hemoglobin (Hb) were purchased from Sigma Chemical Co. (St. Louis, MO, USA). Glutaraldehyde (GA) was purchased from Beijing Chemical Reagent Co. (Beijing, China). Hexanethiol (96%, HT), gold chloride (1%, $HAuCl_4$), ammonia ($NH_3 \cdot H_2O$), O-phenylenediamine (OPD), M-phenylenediamine (MPD) and P-phenylenediamine (PPD) were obtained Shanghai Chemical Reagent Co. (Shanghai, China). 3,4,9,10-Perylenetetracarboxylic dianhydride ($C_{24}H_8O_6$, PTCDA) was bought from Lian Gang Dyestuff Chemical Industry Co. Ltd. (Liaoning, China). L-cysteine (L-cys) was obtained from Chengdu kelong chemical Industry. All oligonucleotides were synthesized by Sangon Biotech. Co. Ltd. (Shanghai, China) with the sequences of the oligonucleotides as followed:

Thrombin aptamer (TB): 5'-NH_2-$(CH_2)_6$-GGTTGGTGTGGTTGG-3'

Complementary thrombin binding aptamers (CTBA): 5'-NH_2-$(CH_2)_6$-CCAACC ACACCAACC-3'

20 mM Tris-HCl buffer (pH 7.4) containing 140 mM NaCl, 5 mM KCl and 1 mM $MgCl_2$ was used to prepare aptamer and thrombin (TB) solutions. Phosphate buffered solution (PBS) (pH 7.0) was prepared using 10 mM Na_2HPO_4, 10 mM KH_2PO_4 and 2 mM $MgCl_2$ as working buffer. The human serum samples were acquired from the Ninth people's Hospital of Chongqing, China. All other chemicals were of analytical grade and used as received. Ultrapure water was employed throughout this study.

1.2 Instrumentations

Cyclic voltammetry (CV) was performed on a CHI 660D electrochemical workstation (Shanghai Chenhua Instrument, China). A conventional three-electrode system was used for all electrochemical measurements: a platinum wire as auxiliary electrode, the modified glassy carbon electrode (GCE, Φ = 4mm) as working electrode, and a saturated calomel electrode (SCE) as reference electrode. CVs of the electrode fabrication were performed in PBS (pH 7.0) with a scanning potential from -0.8 to 0.1 V at a scan rate of 100 mV/s. The scanning electron micrographs were taken with scanning electron microscope (SEM, S-4800, Hitachi, Japan). All calculations for the energies of hydrogen bonding were implemented with the Gaussian 09 program. Full geometry optimizations were run to locate all of the stationary points, using the B3LYP method[1] with 6-311++G (d, p) basis set for C, H,

N, and O atoms[2] namely B3LYP/6-311++G (d, p), aug-cc-pvtz. The effect of the water solvent was included by embedding these species in a polarizable continuum solvent model using the iterative integral equation formalism polarized continuum model (IEF-PCM) formalism[3] with a water dielectric constant of 78.39, an ionic strength of 0, and the United Atom Topological Model (UAKS) parameter set. Meanwhile, the stability of the density function theory (DFT) wave function was tested.[4] If an instability was found, the wave function was reoptimized with appropriate reduction in constraints, and the stability tests and reoptimizations were repeated until a stable wave function was found.[5] Espinosa et al. Group[6] had proposed that the relationship between bond energy E_{HB} and potential energy density $V(r)$ at corresponding the bond critical point (BCP) could be approximately described as $E_{HB}=V(r_{bcp})/2$ for the hydrogen bonding [X-H···O(X=C, N, O)]. We evaluated the energies of hydrogen bonding in our system by this formula with the Multiwfn Software.[7]

1.3 Preparation of PTCA/O-phenylenediamine (PTCA/OPD) nanomaterials

PTCA/OPD nanomaterials was prepared with PTCA as a template by a simple π-π interactions approach. In a typical experiment, PTCA was synthesized from hydrolyzed PTCDA by a modified Caruso method.[8] Then OPD (14 mg) was added in the prepared PTCA aqueous solution, at the same time, 25 μL ammonia ($NH_3 \cdot H_2O$) was also dropped to the mixture solution with magnetic stirring for 24 h at the room temperature. After centrifugated at 12000 rpm for 20 min to remove surplus OPD, the sediments of the resulted PTCA/OPD nanomaterials were respectively resuspended in

ultrapure water and stored at 4 ℃ for further use. The control nanomaterials including PTCA/M-phenylenediamine (PTCA/MPD) and PTCA/P-phenylenediamine (PTCA/PPD) nanomaterials were prepared with the same method.

2 Results and discussion

2.1 Characteristics of the different nanomaterials

The sizes and morphologies of different nanomaterials were characterized by scanning electron microscope (SEM). As shown in Fig. S1A, typical SEM image of PTCA was observed. The uniform cylindrical-like morphology suggested the successful preparation of PTCA. However, after combining with OPD to form nanomaterials, the morphology showed irregular flat lump with large specific surface area (Fig. S1B) compared to the original PTCA particles. The change of morphology may contribute to the π-π interactions and hydrogen bonding between PTCA and OPD enhancing the delocalize charge and resonance energy effectively. While the Fig. S1C and Fig. S1D showed the images of the PTCA/MPD and PTCA/PPD, which were different from the PTCA/OPD and displayed flat rod-like structures. The reason was the force of forming π-π interactions or hydrogen bonding between PTCA and MPD or PPD more difficult. These results demonstrated that the strength of π-π interactions and hydrogen bonding may influence morphologies of PTCA/OPD, PTCA/MPD and PTCA/PPD.

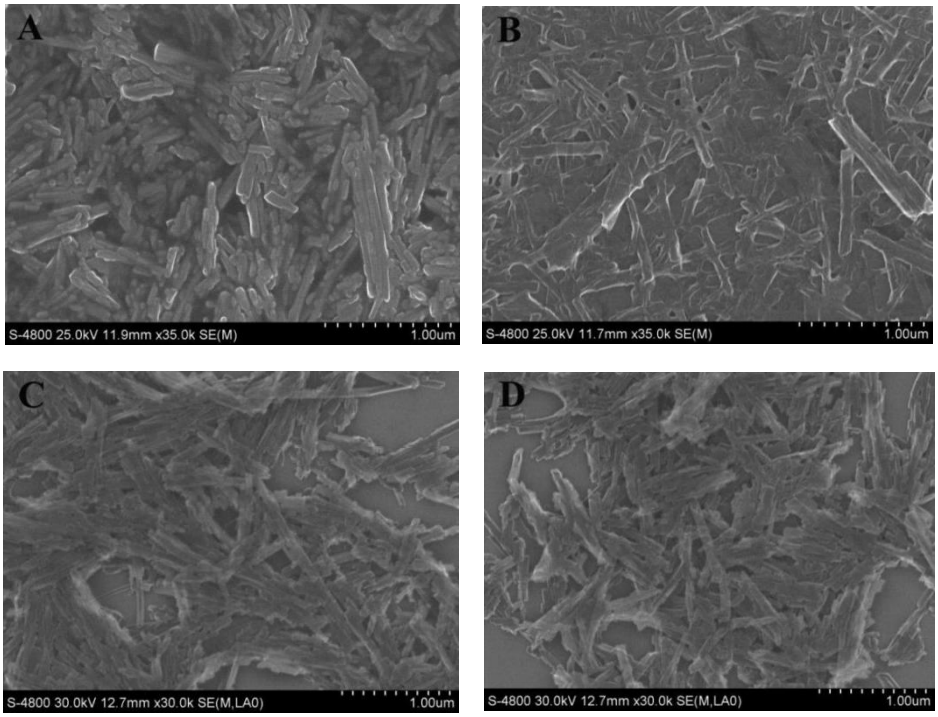

Fig. S1 The SEMs of PTCA (A), PTCA/OPD (B), PTCA/MPD (C) and PTCA/PPD (D).

Additionally, X-ray photoelectron spectroscopy (XPS) analysis provided more detail information for the prepared PTCA/OPD nanomaterials. As shown in Fig. S2, the obvious peaks of C, O and N appeared in the XPS survey spectrum at the same time, verifying that PTCA/OPD nanomaterials were successfully synthesized *via* π-π interactions and hydrogen bonding.

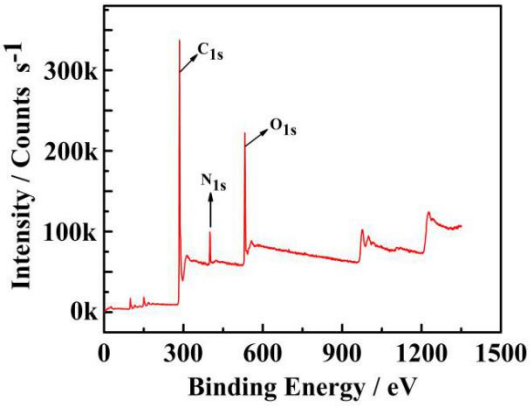

Fig. S2 XPS of PTCA/OPD.

2.2 The electrochemical signal of PTCA/MPD, PTCA/PPD

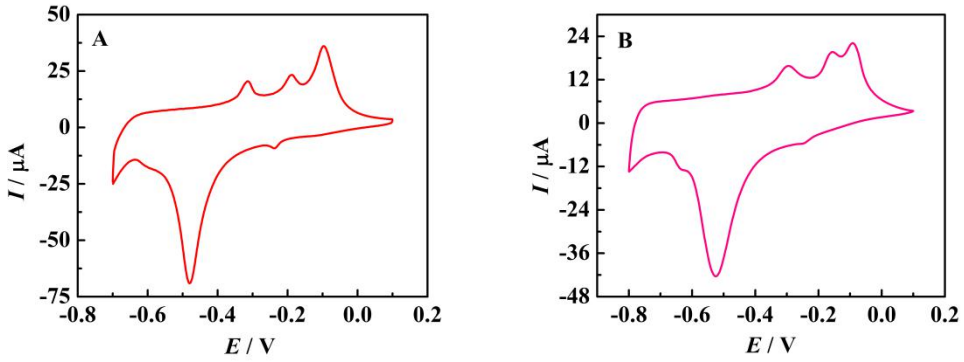

Fig. S3 The redox peaks of PTCA with the ratio for MPD and $NH_3 \cdot H_2O$ (A), PPD and $NH_3 \cdot H_2O$ (B) was 0.576 respectively.

2.3 Electrochemical redox behavior of PTCA/OPD nanomaterials

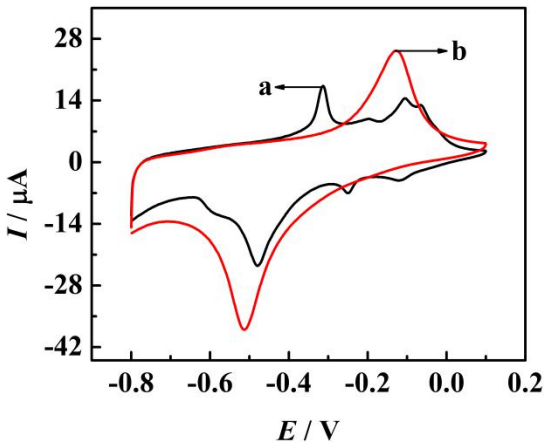

Fig. S4 The redox peaks of PTCA (a) and the redox peaks of PTCA/OPD (b).

In order to demonstrate that PTCA and OPD would appear a well-defined redox peaks *via* π-π interactions and hydrogen bonding, PTCA and PTCA/OPD nanomaterials were directly immobilized on the electrode surfaces. And then, both of them were subjected to cyclic voltammetry (CV) analysis in 0.10 M PBS (pH 7.0) respectively. As shown in Fig. S4, PTCA showed miscellaneous redox peaks (line a) in the potential region from -0.8 to 0.1 V because of the desirable organic electronics of PTCA. However, it was significant that the formation of PTCA/OPD nanomaterials

showed a pair of well-defined redox peaks (line b), which contributed to the π-π interactions or hydrogen bonding between PTCA and OPD, leading to increase the delocalize charge and resonance energy effectively with bringing about a remarkable synergistic action to form a pair of well-defined redox peaks.

2.4 The investigation for the effect of pH and pOPD on the electrochemical signal of PTCA

Due to the fact that the redox peaks of poly-OPD (pOPD) may interfere the redox peaks of PTCA, we investigated the conductive of pOPD electrodeposited in a solution containing 5mM of OPD in acetate buffer (pH 7.0) at a potential of -0.8-0.2 V for 15min.[9] At the same time, the control experiment was performed in a solution containing 5 mM OPD in H_2SO_4 (pH 2.47) under the same condition.[10] As shown in Fig. S5, no obvious redox peaks appeared (line a) in our work condition (pH 7.0), which ascribed to the fact that at neutral or basic pH, OPD oligomers were less protonated, allowing strong π-π interactions to occur and leading to the self-assembly of pOPD with long and non-conductive microstructures. However, at acidic pH, OPD oligomers were comparatively more protonated, and therefore electrostatic repulsive forces resulted in the formation of pOPD with small self-assembled microstructures,[11] which became conductive when doped with protons (H^+) at acidic pH 2.47 (line b). This phenomenon strongly supported to the claim that the well-defined redox peaks of PTCA/OPD nanomaterials was not the redox peaks of pOPD, but resulted from the fact that the synergitic action coupling the π-π interactions with the hydrogen bonding between PTCA and OPD could increase delocalize charge and resonance energy

effectively, leading to the miscellaneous redox peaks of PTCA tend into a pair of well-defined redox peaks.

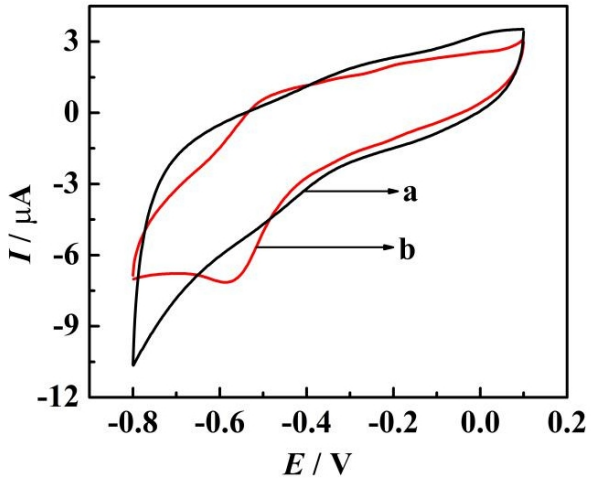

Fig. S5 The peaks of pOPD (pH 7.0, line a), and the redox peaks of pOPD (pH 2.47, line b).

Furthermore, pH was another possibility to effect the redox peaks of the PTCA. Therefore, the potential influence of pH toward the redox peaks of PTCA was investigated by detecting the CV responses of the electrodes incubated the following PTCA with different pH: pH (2-3), pH (4-5), pH (6-7), pH (8-9), pH (9-10) and pH (10-11). From the results showed in Fig. S6, the electrochemical signal of the PTCA was influenced with different pH. Whereas the shapes for redox peaks of the PTCA were not effected by different pH. These results demonstrated that the well-defined redox peaks of PTCA/OPD were rather the resonance energy and delocalize charge effectively between PTCA and OPD than the influence of pH to PTCA.

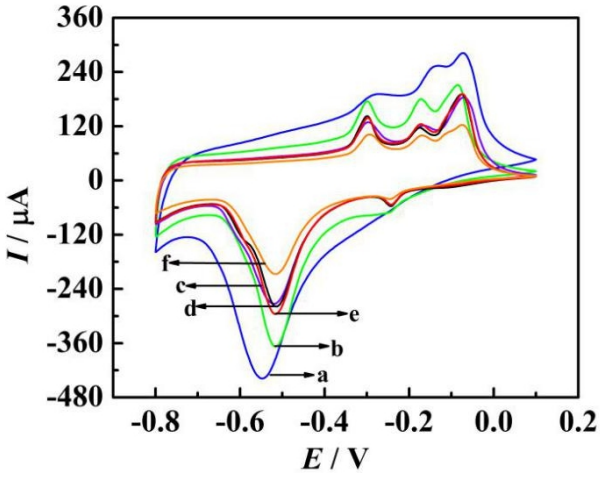

Fig. S6 The redox peaks of PTCA with different pH: pH (2-3) (a), pH (4-5) (b), pH (6-7) (c), pH (8-9) (d), pH (9-10) (e), pH (10-11) (f).

2.5 Electrochemical characterization of the aptasensor

To characterize the fabrication process of the proposed aptasensor, CV measurements were performed to provide the evidence for the interface properties of surface-modified electrodes. CVs of different modified electrodes investigated by CV measurements in 1.0 mL PBS solution were acquired (Fig. S7), no obvious redox peaks were exhibited for the pretreated bare GCE (Fig. S7, curve a) as the lack of electroactive probe. The well-defined redox peaks appeared (Fig. S7, curve b) after the electrode surface was immobilized with a film of PTCA/OPD. Owing to the conductivity of nano-Au, the peaks current markedly increased (Fig. S7, curve c). After TBA assembly of the modified electrode, the current signal decreased (Fig. S7, curve d) which attributed that the electron transfer tunnel was blocked, leading to the decrease of current signal. As expected, the peak current (Fig. S7, curve e) was further decreased by employing HT to block nonspecific sites. However, the introduction of CTBA-MB complex resulted in increase of the current signal, which revealed the new

discovery that MB could perfectly catalyze the PTCA/OPD (Fig. S7, curve f). Finally, the decrease of the peak current was observed in the presence of the TB, because the TBA combined with TB forming G-quartet to replace the CTAB/MB complex (Fig. S7, curve g).

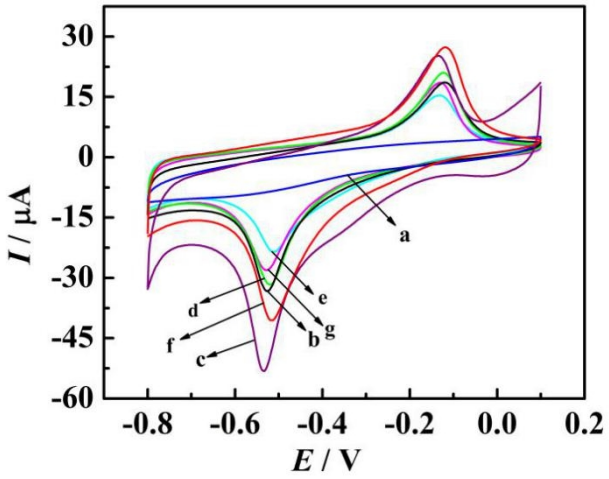

Fig. S7 The CV of the stepwise modified electrodes: CV of bare GCE (a); GCE-PTCA/OPD (b); GCE-PTCA/OPD-Au (c); GCE-PTCA/OPD-Au-TBA (d); GCE-PTCA/OPD-Au-TBA-HT (e); GCE-PTCA/OPD-Au-TBA-HT-CTBA/MB (f).

2.6 The CV response and calibration curves for the electrochemical aptasensor without MB

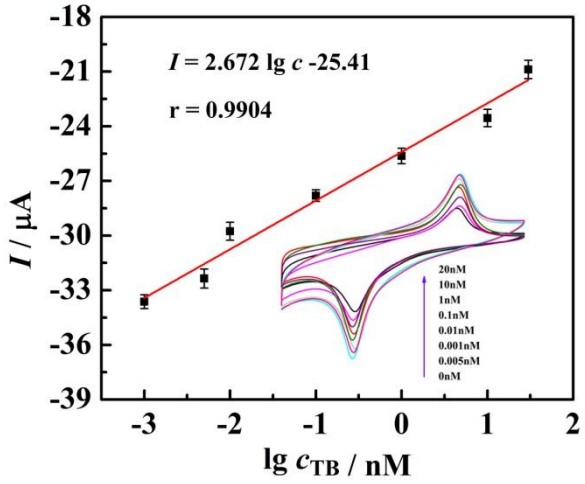

Fig. S8 The calibration plots of the oxidation peak current response versus the logarithm concentration of TB for the contrast aptasensor without MB. The insets show the CVs of the redox peaks at different concentrations in 1.0 mL 0.1 M PBS (7.0).

2.7 Specificity and analytical application of the proposed electrochemical aptasensor

To evaluate the specificity of the proposed electrochemical aptasensor, we measured the system with other biomolecules in human serum, such as, bovine serum albumin (BSA), hemoglobin (Hb), human IgG, and lysozyme (L-cys) under the same experimental conditions. We could see from Fig. S9, high signal was obtained only when the specific protein TB was tested, whereas the electrochemical signals could almost be negligible in the presence of other potential interferences. The presence of the target analyte (TB, 1 nM) resulted in the dramatic increasing of the current. Significantly, high concentration (100 nM) of BSA, IgG, Hb and L-cys did not affect the large current change. These results demonstrated that the proposed aptasensor was specific to TB and possessed high specificity. The stability of the aptasensor was

investigated every 7 days for long-term storage at 4 ℃. The aptasensor less than 4.2 % of its initial current after 7 days storage, and it kept 90.4 % of the initial current after 28 days storage, suggesting that the proposed aptasensor had acceptable stability. Moreover, the reproducibility of the aptasensor was investigated by analysis of the same concentration of TB (1 nM) using intra- and inter-assay coefficients of variation under the same conditions, and a relative standard deviation (RSD) of 4.6 % was acquired with various electrodes. Similarly, the present aptasensor using the same one electrode was repeated for four measurements with 1 nM TB, a RSD of 6.3% was obtained, suggesting that the proposed aptasensor had good reproducibility.

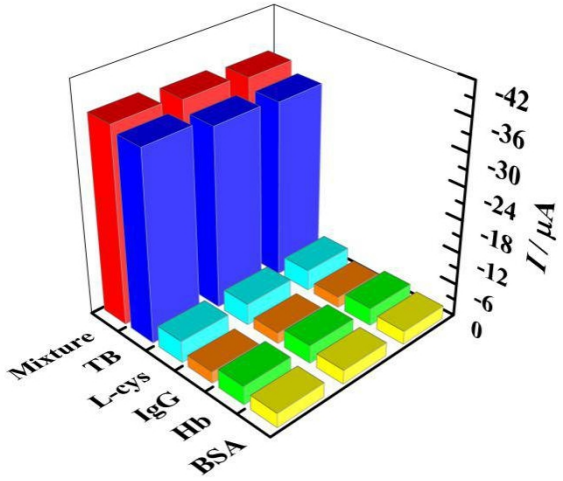

Fig. S9 Selectivity investigation compared with different targets: Mixture (1 nM TB + 100 nM BSA + 100 nM Hb + 100 nM L-cys), TB (1 nM), L-cys (100 nM), IgG (100 nM), Hb (100 nM), BSA (100 nM).

Table S1. Calculated Energies of Hydrogen Bonding (kJ/mol)

E/(kJ/mol)	Bond Lengths of Hydrogen Bonding	
PTCA/OPD	1.996/NH···O=C	1.745/OH···NH
	-20.5	-55.8
PTCA/pOPD	2.239/NH···O=C	2.279/NH···O=C
	-111.7	-97.6

*The calculated energies of hydrogen bonding used the formula $E_{HB}=V(r_{bcp})/2$. *E and V*(*r*) were represented the energies of hydrogen bonding and potential energy density respectively.

Table S2. Measurement of TB added to human blood serum (*n* = 3) with the prepared aptasensor

Sample	Added thrombin/nM	Found thrombin/nM	Recovery/%	RSD/%
1	0.1	0.09247	92.47	3.8
2	1.0	1.068	106.8	4.3
3	10.0	9.832	98.32	4.9
4	20.0	19.84	99.2	5.5
5	50.0	50.28	100.6	6.2

Table S3. Comparisons of proposed aptasensor with other same detection methods for thrombin analysis

Analytical method	Linear range/nM	Detection limit	Ref.
CV	0.001~5	0.12 pM	[12]
CV	0.01~100	10 pM	[13]
CV	0.1~10.0	31.3 pM	[14]
CV	0.00014~0.056	0.14 pM	[15]
CV	1~100	0.1 nM	[16]
CV	0.0001~30	0.05pM	The work

References

1 C. Lee, W. Yang and R. G. Parr, *Phys. Rev. B*, 1988, **37**, 785-789.

2 A. D. Mclean and G. S. Chandler, *J. Chem. Phys.*, 1980, **72**, 5639-5648.

3 C. Adamo and V. Barone, *J. Chem. Phys.*, 1999, **110**, 6158-6170.

4 R. Bauernschmitt and R. Ahlrichs, *J. Chem. Phys.*, 1996, **104**, 9047-9052.

5 R. Seeger and J. A. Pople, *J. Chem. Phys.*, 1977, **66**, 3045-3050.

6 T. Lu, F. W. Chen and J. Comput, *Anal. Chem.*, 2012, **33**, 580-592.

7 E. Espinosa, E. Molins and C. Lecomte, *Chem. Phys. Lett.*, 1998, **285**, 170-173.

8 F. Caruso, E. Rodda and D. N. Furlong, *Anal. Chem.*, 1997, **69**, 2043-2049.

9 R. Garjonyte and A. Malinauskas, *Sen. and Act. B*, 1999, **56**, 85-92.

10 J. W. Long, C. P. Rhodes, A. L. Young and D. R. Rolison, *NANO Lett.*, 2003, **3**, 1155-1161.

11 A. Asati, D. Lehmkuhl, D. Diaz and J. M. Perez, *Langmuir*, 2012, **28**, 13066-13071.

12 G. F. Jie and J. X. Yuan, *Anal. Chem.*, 2012, **84**, 2811-2817.

13 Y. Du, B. L. Li, H. Wei, Y. L. Wang and E. K. Wang, *Anal. Chem.*, 2008, **80**, 5110-5117.

14 H. X. Chang, L. H. Tang, Y. Wang, J. H. Jiang and J. H. Li, *Anal. Chem.*, 2010, **82**, 2341-2346.

15 M. A. Rahman, J. I. Son, M. S. Won and Y. B. Shim, *Anal. Chem.*, 2009, **81**, 6604-6611.

16 Y. C. Fu, C. Zou, L. J. Bu, Q. J. Xie and S. Z. Yao, *ACS Appl. Mater. Interfaces*, 2013, **5**, 934-939.